Available online at www.sciencedirect.com
SCIENCE DIRECT®
Bioorganic & Medicinal Chemistry 13 (2005) 301–312
Bioorganic & Medicinal Chemistry

Structure-based discovery of human L-xylulose reductase inhibitors from database screening and molecular docking

Vincenzo Carbone,[a] Syuhei Ishikura,[b] Akira Hara[b] and Ossama El-Kabbani[a,*]

[a]*Department of Medicinal Chemistry, Victorian College of Pharmacy, Monash University, Parkville, Victoria 3052, Australia*
[b]*Laboratory of Biochemistry, Gifu Pharmaceutical University, Mitahora-higashi, Gifu 502-8585, Japan*

Received 9 August 2004; revised 10 October 2004; accepted 11 October 2004
Available online 5 November 2004

Abstract—Human L-xylulose reductase (XR) is an enzyme of the glucuronic acid/uronate cycle of glucose metabolism and is a possible target for treatment of the long-term complications of diabetes. In this study we utilised the molecular modelling program DOCK to analyse the 249,071 compounds of the National Cancer Institute Database and retrieved those compounds with high predicted affinity for XR. Several carboxylic acid-based compounds were tested and shown to inhibit XR. These included nicotinic acid (IC_{50} = 100 μM), benzoic acid (IC_{50} = 29 μM) and their derivatives. These results extend and improve upon the activities of known, commercially available inhibitors of XR such as the aliphatic fatty acid *n*-butyric acid (IC_{50} = 64 μM). To optimise the interaction between the inhibitor and the holoenzyme, the program GRID was used to design de novo compounds based on the inhibitor benzoic acid. The inclusion of a hydroxy-phenyl group and a phosphate to the benzoic acid molecule increased the net binding energy by 1.3- and 2.4-fold, respectively. The resultant compounds may produce inhibitors with improved specificity for XR.
© 2004 Elsevier Ltd. All rights reserved.

1. Introduction

Human L-xylulose reductase (XR, EC 1.1.1.10) catalyses the NADPH-linked reduction of L-xylulose into xylitol.[1] The enzyme also reduces several types of pentoses, tetroses, trioses, ketones and α-dicarbonyl compounds.[2,3] The reductase activities of the mouse, rat, hamster and human XRs are inhibited by short chain fatty acids and their derivatives, of which hexanoic acid and *n*-butyric acid are the most potent inhibitors, showing IC_{50} values of 0.10 and 0.064 mM, respectively, for human XR.[2]

XR belongs to a group of enzymes in the glucuronic acid/uronate cycle of glucose metabolism,[4–7] a pathway that accounts for approximately 5% of the total glucose catabolised per day in humans.[8] The glucuronic acid/uronate cycle is very active in the kidney[2] and provides an important source of uridine diphosphate glucose that is used in the synthesis of glycogen[9] and in the formation of mucopolysaccharides of the basement membrane.[10–12] Recently, XR was demonstrated to be a ubiquitous protein with high expression in the liver and kidney of human, hamster and guinea pig, and was shown to localise specifically in the inner membranes of the proximal and renal tubules of human and murine kidneys.[2,3] These observations support a secondary role for XR as a detoxification enzyme, in a process that targets α-dicarbonyl compounds formed in tissue in the liver or ingested as part of food or beverage.[13] This includes the reduction of methylglyoxal, an α-dicarbonyl compound involved in the formation of advanced glycation end products that can induce cellular degradation and may have a role in the development of diabetic complications and atherosclerosis.[14] The reduction of sugars such as threoses by XR is also important as they are known to generate highly reactive superoxide anions in vivo.[15] In short term and long term diabetic rat models[6] and in humans with diabetes,[7] the activity of XR and the utilisation of glucose via this pathway increased resulting in a greater incorporation of carbohydrate derivatives into the basement membrane of tissues within the kidney[16] and a massive increase in glycogen content in this organ. Over time, abuse of such pathways contributes to glomerular basement membrane lesions and thickening in the kidney, which then causes sclerotic disorders in the blood vessels and tissues[17] and can ultimately lead to the progressive pathologies associated with diabetes mellitus and the loss of kidney function. XR is therefore

Keywords: Molecular modelling; Drug design.
* Corresponding author. Tel.: +61 3 9903 9691; fax: +61 3 9903 9582; e-mail: ossama.el-kabbani@vcp.monash.edu.au

0968-0896/$ - see front matter © 2004 Elsevier Ltd. All rights reserved.
doi:10.1016/j.bmc.2004.10.030

a target for understanding the aetiology of diabetic complications and an important determinant for the metabolic responses to diabetes, especially within the kidney.

New classes of compounds are continuously being produced and tested for their efficacy as drugs. In recent years, the pharmaceutical industry has helped develop means to increase the success rate of discovery of new and novel inhibitors away from the predominantly random and expensive process of screening large synthetic or natural product libraries in vitro.[18,19] Here we report the utilisation of a computational-based approach to produce a reliable and inexpensive means of identifying new and potentially active inhibitors for XR prior to in vitro testing.[20,21] The National Cancer Institute (NCI) database contains approximately 250,000 compounds that are freely available for download (http://cactus.nci.nih.gov).[22–25] Used in conjunction with the program DOCK[26] and the crystal structure of XR,[27] a functional search model for the discovery of new inhibitors was formulated and compounds commercially available were selected and tested for inhibitory potency on XR. Following database docking, molecular modelling techniques were used for the de novo design of compounds[28] based on the most potent of the newly discovered inhibitors of XR.

2. Results and discussion

2.1. Database refinement

To prepare the NCI database to initiate a search for new inhibitors of XR we first needed to modify the database so it was suitable for compound screening. This process involved the manual editing and excising compounds due to occasional errors in the mol2 format of some compounds or because others were too large to be surfaced by the DOCK program.[29] In addition to this, compounds that are chemically toxic (i.e., containing atoms such as Pt, Hg, Pu, Cr or Ir) were also removed. Approximately 12,185 compounds were deleted initially, at an attrition rate of 4.89%.

The DOCK program read 236,886 compounds, of which 229,725 compounds were docked successfully. The disparity between the observed number of compounds and those utilised by DOCK is due to the chemical and physical filters utilised by the program. This includes ignoring compounds that contained heavy atoms such as Zn, Al, Au or Ag, or compounds that had too many or incorrectly assigned rotatable bonds. These filters help to eliminate compounds whose components may be associated with poor chemical stability or toxicity.[21] Overall, 25,000 compounds were selected by DOCK to have the highest energy score, of which 1014 appeared within the active site of XR (~0.4% of the total NCI database). Charges and force field potentials were assigned to the 1014 compounds and the DOCK process repeated.

By utilising DOCK to screen the NCI database, we produced large volumes of data and limited means by which we can discriminate amongst compounds to test. It has been well established that consensus between geometric placement of the compound within the active site of the protein and DOCK energy score is a means by which compounds can be selected.[20] Therefore potential inhibitor candidates were trialled based on the highest energy score, proximity to the C4 carbon of $NADP^+$ and the catalytic residues (Ser136 and Tyr149) of XR, and commercial availability. The majority of compounds subsequently tested (Table 1) were acids containing a carboxylate group (COO^-). This also included benzoic acid and nicotinic acid-based derivatives. These compounds proved to have the highest energy scores and were generally the easiest to find amongst commercial distributors.

2.2. Database analysis

Since short chain acids have been known to inhibit XR[2], it was prudent to extend these results in the hope of finding similar groups of small, relatively potent inhibitors. The majority of compounds tested therefore were carboxylic acid-based aliphatic compounds, many of which showed no substantial inhibitory effect on XR (namely compounds **1**–**17**, **20**, **22** and **24**). The inability of compounds such as these to inhibit XR is most likely due to their highly hydrophilic nature. The occurrence of a carboxylic, sulfonic, hydroxy or basic substituents such as an amino group increases the hydrophilicity of the compound thereby limiting their ability to make the necessary tight binding and hydrophobic interactions with residues within the active site. In vitro, compounds such as these may suffer from a high rate of desolvation into the aqueous environment at physiological pH and might therefore show poor activity in vivo. In addition to its highly hydrophilic nature, inhibitor candidates such as 3-hexenedioic acid (compound **2**) and maleic acid (compound **12**), which have double-bonded carbon atoms, proved to be unable to make adequate, modelled interactions with active site residues. This may have caused the poor to undetectable levels of XR inhibition in vitro. This is especially true for 3-cyano and 4-cyanopyridine (compounds **30** and **31**, respectively), which have no rotatable bonds and therefore failed to adopt substantial or multiple interactions with active site residues.

n-Butyric acid is known to inhibit XR by binding the substrate-interacting residues Gln137, Leu143 and His146 of the rat enzyme.[2,30] Similarly, computer modelling studies based on a model of XR and butyric acid[31] demonstrated the ability of the inhibitors to form contacts with Val143 and the catalytic residues Ser136 and Tyr149. Therefore we may identify new inhibitors for human XR by utilising *n*-butyric acid-based derivatives and analysing their associations with the active site residues Gln137, Val143 and His146. 4-Aminobutanoic acid and 4-bromobutyric acid (compounds **20** and **21**, respectively) are two such compounds, which differ from *n*- butyric acid by the addition of a hydrophilic amino group and lipophilic halogen. Compounds **20** and **21** possessed similar DOCK energy scores and appeared within the active site in a comparable fashion with small

Table 1. Docking scores and inhibitory activities of compounds sourced after NCI database docking with the crystal structure of XR

Compounds	DOCK energy score (kcal)	Percentage inhibition	IC_{50}	Proximity to catalytic residues
1 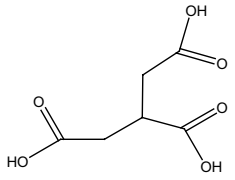 **Tricarballylic acid**	−42.94	7% at 10 mM	NT[a]	Ser136: 2.98 Å Tyr149: 2.82 Å $NADP^+$: 3.29 Å
2 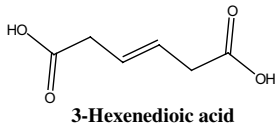 **3-Hexenedioic acid**	−36.96	No detectable inhibitory effect	—	Ser136: 2.92 Å Tyr149: 3.11 Å $NADP^+$: 3.06 Å
3 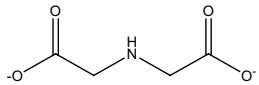 **Disodium iminodiacetate**	−36.66	No detectable inhibitory effect	—	Ser136: 3.15 Å Tyr149: 2.82 Å $NADP^+$: 3.32 Å
4 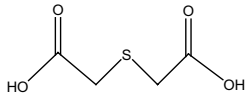 **Thiodiglycolic acid**	−36.58	28% at 10 mM	NT[a]	Ser136: 2.83 Å Tyr149: 2.75 Å $NADP^+$: 3.32 Å
5 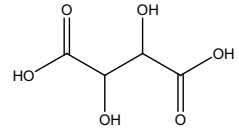 **2,3-Dihydroxysuccinic acid**	−35.64	17% at 10 mM	NT[a]	Ser136: 2.90 Å Tyr149: 2.95 Å $NADP^+$: 3.14 Å
6 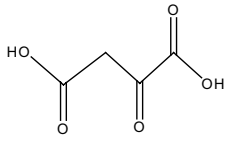 **2-Oxosuccinic acid**	−35.95	56% at 10 mM	NT[a]	Ser136: 3.91 Å Tyr149: 3.56 Å $NADP^+$: 3.14 Å
7 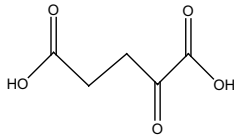 **2-Oxopentanedioic acid**	−35.38	57% at 10 mM	NT[a]	Ser136: 3.07 Å Tyr149: 3.68 Å $NADP^+$: 3.9 Å
8 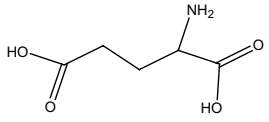 **Glutamic acid**	−34.45	9% at 10 mM	NT[a]	Ser136: 2.80 Å Tyr149: 2.69 Å $NADP^+$: 3.39 Å
9 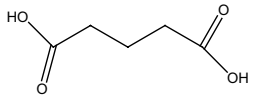 **Glutaric acid**	−34.07	No detectable inhibitory effect	—	Ser136: 3.15 Å Tyr149: 2.83 Å $NADP^+$: 3.85 Å
10 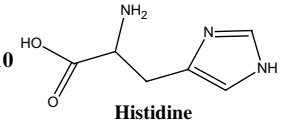 **Histidine**	−33.49	4% at 10 mM	NT[a]	Ser136: 2.96 Å Tyr149: 2.69 Å $NADP^+$: 2.93 Å

(*continued on next page*)

Table 1 (*continued*)

Compounds	DOCK energy score (kcal)	Percentage inhibition	IC_{50}	Proximity to catalytic residues
11 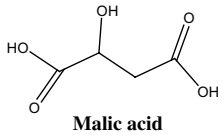 **Malic acid**	−33.42	17% at 10 mM	NT[a]	Ser136: 2.91 Å Tyr149: 3.05 Å $NADP^+$: 3.59 Å
12 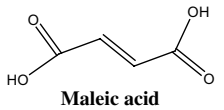 **Maleic acid**	−33.05	7% at 10 mM	NT[a]	Ser136: 3.10 Å Tyr149: 4.55 Å $NADP^+$: 3.54 Å
13 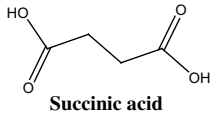 **Succinic acid**	−32.50	7% at 10 mM	NT[a]	Ser136: 3.56 Å Tyr149: 2.92 Å $NADP^+$: 3.36 Å
14 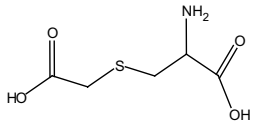 **S-(carboxymethyl) cysteine**	−31.83	No detectable inhibitory effect	—	Ser136: 2.84 Å Tyr149: 3.38 Å $NADP^+$: 3.04 Å
15 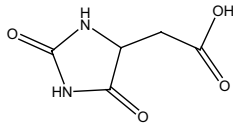 **5-Hydantoinacetic acid**	−31.56	8.1% at 10 mM	NT[a]	Ser136: 2.94 Å Tyr149: 3.43 Å $NADP^+$: 3.29 Å
16 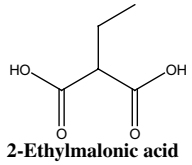 **2-Ethylmalonic acid**	−31.30	62.1% at 10 mM	NT[a]	Ser136: 2.69 Å Tyr149: 3.04 Å $NADP^+$: 3.07 Å
17 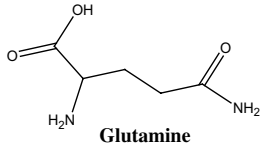 **Glutamine**	−30.08	11% at 10 mM	NT[a]	Ser136: 3.19 Å Tyr149: 3.34 Å $NADP^+$: 3.20 Å
18 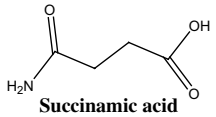 **Succinamic acid**	−29.59	77.46% at 10 mM	1.45 mM	Ser136: 3.20 Å Tyr149: 3.31 Å $NADP^+$: 3.46 Å
19 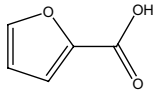 **2-Furoic acid**	−27.18	87% at 10 mM	0.242 mM	Ser136: 4.92 Å Tyr149: 3.55 Å $NADP^+$: 3.26 Å
20 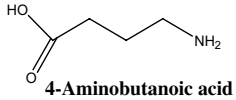 **4-Aminobutanoic acid**	−26.87	No detectable inhibitory effect	—	Ser136: 3.32 Å Tyr149: 2.90 Å $NADP^+$: 3.21 Å
21 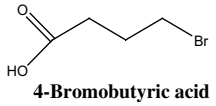 **4-Bromobutyric acid**	−26.73	86.4% at 10 mM	0.150 mM	Ser136: 3.88 Å Tyr149: 3.51 Å $NADP^+$: 3.41 Å

Table 1 (*continued*)

Compounds	DOCK energy score (kcal)	Percentage inhibition	IC_{50}	Proximity to catalytic residues
22 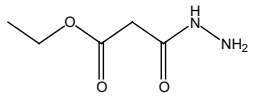 **Ethyl-3-hydrazino-3-oxopropionate**	−26.09	9.16% at 10 mM	NT[a]	Ser136: 2.99 Å Tyr149: 2.97 Å $NADP^+$: 3.03 Å
23 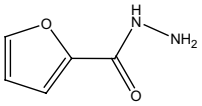 **2-Furohydrazide**	−26.02	81.3% at 10 mM	2.75 mM	Ser136: 3.50 Å Tyr149: 3.25 Å $NADP^+$: 3.08 Å
24 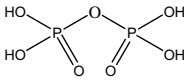 **Pyrophosphoric acid**	−25.62	No detectable inhibitory effect	—	Ser136: 3.11 Å Tyr149: 2.90 Å $NADP^+$: 3.01 Å
Nicotinic acid based derivatives				
25 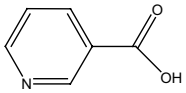 **Nicotinic acid**	−27.87	100% at 10 mM	0.100 mM	Ser136: 4.86 Å Tyr149: 2.84 Å $NADP^+$: 3.20 Å
26 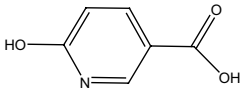 **6-Hydroxynicotinic acid**	−28.37	No detectable inhibitory effect	—	Ser136: 4.09 Å Tyr149: 2.86 Å $NADP^+$: 3.29 Å
27 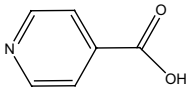 **Isonicotinic acid**	−27.49	100% at 10 mM	0.420 mM	Ser136: 4.38 Å Tyr149: 3.28 Å $NADP^+$: 2.88 Å
28 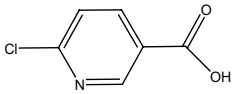 **6-Chloronicotinic acid**	−26.81	51.1% at 1.25 mM	1.22 mM	Ser136: 2.78 Å Tyr149: 4.15 Å $NADP^+$: 3.72 Å
29 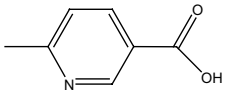 **6-Methylnicotinic acid**	−22.67	15.82% at 1.25 mM	NT[a]	Ser136: 3.29 Å Tyr149: 3.95 Å $NADP^+$: 3.27 Å
30 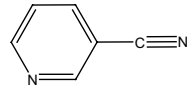 **3-Cyanopyridine**	−17.19	No detectable inhibitory effect	—	Ser136: 4.50 Å Tyr149: 4.51 Å $NADP^+$: 3.80 Å
31 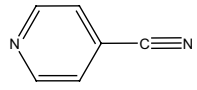 **4-Cyanopyridine**	−16.96	No detectable inhibitory effect	—	Ser136: 4.32 Å Tyr149: 4.63 Å $NADP^+$: 3.74 Å
32 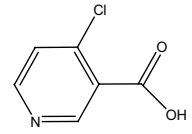 **2-Chloronicotinic acid**	−14.07	67.7% at 1.25 mM	0.313 mM	Ser136: 2.82 Å Tyr149: 5.08 Å $NADP^+$: 3.43 Å
Benzoic acid based derivatives				
33 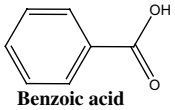 **Benzoic acid**	−20.21	79.97% at 1.25 mM	0.029 mM	Ser136: 3.31 Å Tyr149: 5.28 Å $NADP^+$: 3.59 Å

(*continued on next page*)

Table 1 (*continued*)

Compounds	DOCK energy score (kcal)	Percentage inhibition	IC_{50}	Proximity to catalytic residues
34 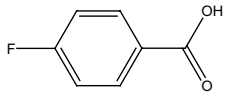 **4-Fluorobenzoic acid**	−26.94	76.82% at 1.25 mM	0.180 mM	Ser136: 2.96 Å Tyr149: 4.02 Å $NADP^+$: 3.52 Å
35 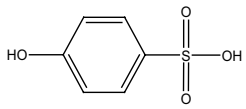 **4-Hydroxybenzenesulfonic acid**	−26.08	4.42% at 10 mM	NT[a]	Ser136: 2.76 Å Tyr149: 4.57 Å $NADP^+$: 3.82 Å
36 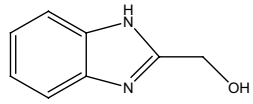 **2-Benzimadazolemethanol**	−26.03	No detectable inhibitory effect	—	Ser136: 4.45 Å Tyr149: 4.81 Å $NADP^+$: 3.40 Å
37 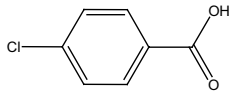 **4-Chlorobenzoic acid**	−25.23	74.6% at 1.25 mM	0.200 mM	Ser136: 2.82 Å Tyr149: 3.88 Å $NADP^+$: 3.43 Å
38 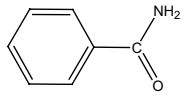 **Benzamide**	−21.58	—	0.095 mM	Ser136: 3.26 Tyr149: 3.53 $NADP^+$: 3.77
39 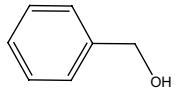 **Benzyl alcohol**	−16.67	38% at 1 mM	NT[a]	Ser136: 4.96 Tyr149: 3.16 $NADP^+$: 3.33

[a] Not tested: unsuitable level of XR inhibition to warrant IC_{50} determination.

variations in distances to active site residues such as Ser136 (3.32 Å/3.88 Å, respectively) and Tyr149 (2.90 Å/3.51 Å, respectively). However, neither compound made van der Waals contacts with Val143 and His146, residues known to bind *n*-butyric acid while engaged in competitive inhibition.[30] This would explain the inability of 4-aminobutanoic acid to act as an inhibitor of XR and may in part be due to a loss in hydrophobic interactions with the side chain of Val143 while 4-bromobutyric acid had a 2.3-fold decrease in inhibitory potency when compared to *n*-butyric acid.

The best of the inhibitors discovered during database mining proved to be those with a lead carboxylic acid (COO^-) attached to a furan, pyridine or benzene ring structure. The most active inhibitors were nicotinic acid (compound **25**, IC_{50} = 100 μM) and benzoic acid (compound **33**, IC_{50} = 29 μM), which were discovered in the initial database search. In the hope of finding inhibitors of equal or greater potency, we utilised the NCI compound browser (http://129.43.27.140/ncidb2/) to search for specific derivatives of benzoic acid and nicotinic acid, which were then downloaded and docked into XR. Although none of the halide or amide derivatives of nicotinic acid and benzoic acid (compounds **28**, **32**, **34**, **37** and **38**) subsequently tested produced more potent inhibitors, each were still able to inhibit XR in the micro to low millimolar range. Cyano-, hydroxy-, methyl- and alcohol-based derivatives (compounds **26**, **29**, **30**, **31**, **36** and **39**) failed to inhibit XR to any significant level. These modelled compounds also failed to make adequate contacts with the catalytic residues of XR.

Benzoic acid has a 3.45-fold greater potency in inhibiting XR in vitro, over nicotinic acid. Given the comparative structure, molecular weight and charged carboxylate group of both compounds, we investigated the intermolecular bonds between enzyme and inhibitor so as to define the necessary interactions that may contribute to the lower IC_{50} value of benzoic acid. The ternary complexes were viewed following minimisation and dynamics analysis. The derivatives of both compounds were also minimised and their intermolecular interactions assessed.

The nicotinic acid–XR ternary complex has a net binding energy of −60.07 kcal/mol (Fig. 1) while benzoic acid makes fewer hydrogen bond contacts within the active site of XR and has a lower net binding energy of −50.71 kcal/mol (Fig. 2). The carboxylate group of nicotinic acid makes hydrogen bond contacts with catalytic

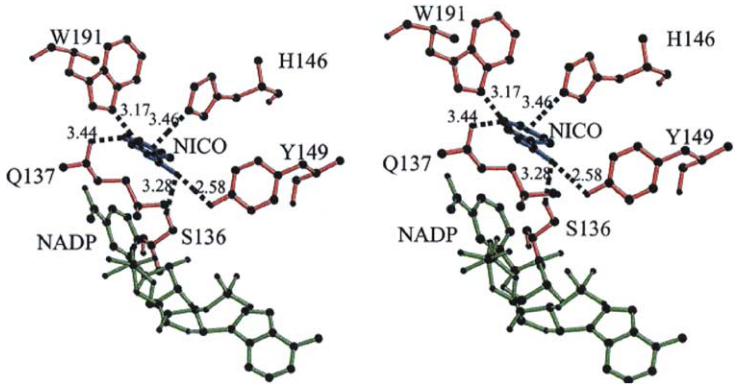

Figure 1. Stereoview of nicotinic acid (blue) modelled into the active site of human XR with $NADP^+$ (green) as the co-enzyme following molecular dynamics calculations. Hydrogen bonds between nicotinic acid and the residues (red) of the active site and their corresponding distances in Å are shown. The figure was prepared using MOLSCRIPT.[41]

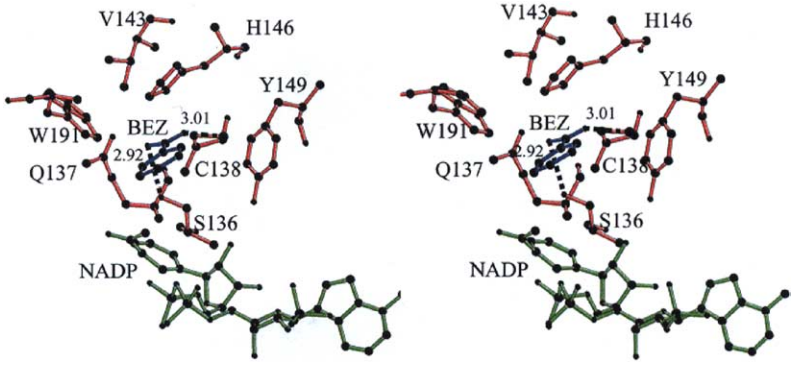

Figure 2. Stereoview of benzoic acid (blue) modelled into the active site of human XR with $NADP^+$ (green) as the co-enzyme following molecular dynamics calculations. Hydrogen bonds between benzoic acid and the residues (red) of the active site and their corresponding distances in Å are shown. The figure was prepared using MOLSCRIPT.[41]

residues Ser136 OG (3.28 Å), Tyr149 OH (2.58 Å), Trp191 NE1 (3.55 Å) and His146 NE2 (3.46 Å), while the pyridine nitrogen forms a hydrogen bond contact with the side chain nitrogen of Gln137 NE2 (2.81 Å). Similarly, the nicotinic acid isomer isonicotinic acid (compound **27**) forms a hydrogen bond contact with the side chain nitrogen of Gln137 NE1 (3.24 Å) via its pyridine nitrogen while the carboxylate group makes hydrogen bond interactions with Tyr149 OH (2.50 Å) and Trp191 NE1 (3.55 Å). The disparity in the number of hydrogen bonds formed may be indicative of the differential ability of both compounds to inhibit XR. The highly inhibitory effect of nicotinic acid is lost when derivatives contain 6-substituents, such as a methyl (compound **29**), a chloro (compound **28**) or a hydroxy group (compound **26**). These derivatives failed to make any or formed weaker interactions with the Gln137 side chain, eliminated the hydrogen bond between the pyridine nitrogen and Gln137 NE1, and perturbed the hydrogen bond interactions with active site residues associated with nicotinic acid. 2-Chloronicotinic acid, while still a potent inhibitor, makes fewer hydrogen bond contacts (Tyr149 OH (3.27 Å) and Thr180 O (3.55 Å)) via its carboxylate group, while the chloride group makes a van der Waals contact with Trp191 NE1 (3.28 Å).

The carboxylate group of benzoic acid forms fewer hydrogen bonds and van der Waals contacts with XR catalytic residues. These included Ser136 OG (2.92 Å) and Cys138 SG (3.01 Å). While not forming many hydrogen bond contacts with the active site residues, benzoic acid does form a π-stacking interaction with the imidazole ring of His146 (4.23 Å). These interactions induce large changes in the side chain and main chain orientation of His146 as well as adjacent residues such as Tyr149. Gross changes such as these within the active site to accommodate the compound may suggest why benzoic acid is more effective inhibitor of XR than nicotinic acid. The derivatives 4-fluorobenzoic acid and 4-chlorobenzoic acid produce similar IC_{50} values for XR although they are far inferior to benzoic acid. This is due to a loss in π-stacking with the imidazole ring of His146, brought about by van der Waals contacts with the side chain sulfur of Met186 and the electronegative halogens fluorine (3.86 Å) and chlorine (3.21 Å), which in turn alters the orientation of the benzene ring within the active site of XR. For benzamide, the formation of a hydrogen bond between the amide group and the side chain nitrogen of Gln137 NE1 (2.99 Å) also disrupts any possible π-stacking interaction with His146.

Overall, π-stacking with the imidazole ring of His146 is an important interaction for benzoic acid and XR, and its loss results in a 3.3-, 6.2- and 6.9-fold decrease in inhibitory activity for benzamide, 4-fluorobenzoic acid and 4-chlorobenzoic acid, respectively. The loss in inhibitory activity for benzamide is not as high because, like nicotinic acid, the loss is alleviated by formation of a hydrogen bond with the active site residue Gln137. These results indicate that the residues Gln137 and His146 in XR form part of the substrate-binding cleft necessary for the undertaking of catalytic reactions and are both important targets when designing inhibitors for XR. Furthermore, they are consistent with the results garnered by Ishikura et al.,[30] which identified several residues of XR, including Gln137 and His146 to actively bind inhibitors.

2.3. Molecular modelling and de novo design

The aromatic ring-based structure of benzoic acid is the most potent of the commercially available inhibitors of XR. The compound competitively inhibits XR but suffers a major drawback in its relatively low in vitro activity when compared to many therapeutic drugs. Benzoic acid would suffer from poor in vivo activity due to the compounds poor pharmacokinetic properties,[32] because it is actively metabolised via glycine conjugation by mitochondrial enzymes and rapidly excreted by the body as hippuric acid in urine.[33–36] Benzene rings and other aromatic systems abound among compounds used as therapeutic agents and these rings play a major role in drugs ranging from providing steric bulk to forming an integral part of the pharmacophore.[37] Given the structure and potency of benzoic acid it became apparent that we should utilise the computer program GRID[28] to produce additional de novo compounds that could be used as possible inhibitors of XR, based on the docked inhibitor. This design process will help us to generate derivatives of benzoic acid that will produce strong modelled interactions with residues within the active site and in turn better inhibitors for XR, which will hopefully possesses none of the detrimental pharmokinectic properties of their parent compound.

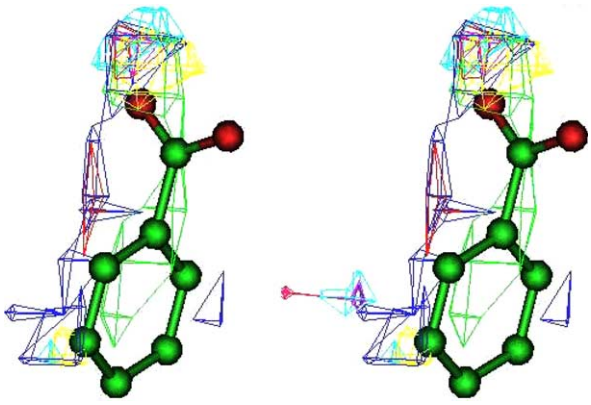

Figure 3. Stereoview showing contours of interaction energies between the active site of XR and phosphate (green), bromine (yellow), methyl (purple), hydroxy phenyl (red), carboxylate (dark blue) and *o*-nitro (light blue) probes with the superimposed benzoic acid (compound **1**). The figure was prepared using InsightII (Biosym Technologies, San Diego, CA, USA).

Table 2. GRID analysis results showing the contour energy levels (kcal) within the active site of XR for the best six probes

Probe	Max. Energy (kcal)
Phosphate	−14.16
Bromine	−8.45
Methyl	−8.44
Hydroxy phenyl	−8.41
Carboxylate	−7.84
o-Nitro	−7.19

For GRID analysis, contour maps were built using steps of 0.4 kcal/mol, where negative energy levels depict regions where ligand binding is most favourable and positive energy levels define the surface of the target. The contour maps were then superimposed on the active site of the docked benzoic acid: XR: $NADP^+$ model. The superimposed benzoic acid structure and the relative position of the favoured probes are shown in Figure 3 and listed in Table 2, with the phosphate probe being the most favoured and the *o*-nitro group the least favoured and resemble closely the probes suggested for butyric acid based derivatives in past molecular modelling studies.[31] The GRID results suggested that the addition of functional groups that were comprised of the probes listed in Table 2 may improve the binding energies of the complex. The designed compounds were then docked manually in the active site of XR based on the orientation of the modelled benzoic acid molecule (compound **33**) so that each probe would be placed in its corresponding favoured region of interaction. Energy minimisation and molecular dynamics calculations were carried out on the 11 compounds shown in Table 3. The calculated binding energies between XR and compounds **33**, **40**–**48** are also listed.

Compounds **40**, **41**, **42**, **44** and **47** had no beneficial effect on the net binding energy to XR when compared to compound **33** (benzoic acid), mainly due to the loss of the negatively charged carboxylate (compounds **40**, **42** and **47**) or the destabilisation of previously modelled side chain interactions with the inhibitor due to the introduction of a bulky halogen or methyl group (compounds **40**, **41**, **42** and **44**). The addition of a carboxylate group to the benzoic acid molecule in compound **43** produced an increase in the net binding energy of the XR–inhibitor complex (1.16-fold) while the most favoured compounds possess an added hydroxy phenyl group (compound **45**; Fig. 4b) or a phosphate group (compound **48**; Fig. 4a), with increases in the net binding energies of the complexes by 1.3- and 2.4-fold, respectively. The enhanced binding energies for the complexes between the XR molecule and both compound **45** (−63.58 kcal/mol) and **48** (−122.64 kcal/mol), compared to benzoic acid (compound **33**; −50.71 kcal/mol), reflected the introduction of new interactions between residues in the active site of the enzyme and the compounds. The phosphate group of phenylphosphonic acid (compound **48**) formed multiple hydrogen bond

Table 3. Protein interaction energies (kcal/mol) calculated between XR residues and compounds **33, 40-48**

Compounds	Structure	Protein interaction energy (kcal/mol)
33	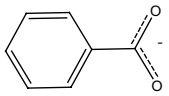 **Benzoic acid**	−50.71
40	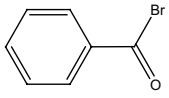 **Benzoyl bromide**	−28.10
41	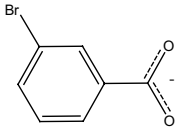 **3-Bromobenzoic acid**	−43.09
42	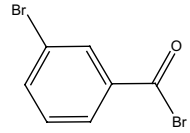 **3-Bromo benzoyl bromide**	−26.39
43	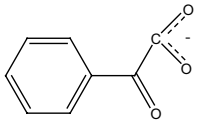 **Phenylglyoxylic acid**	−58.91
44	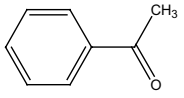 **Acetophenone**	−26.01
45	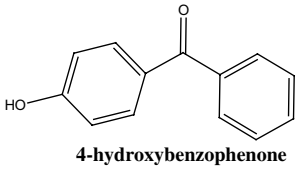 **4-hydroxybenzophenone**	−63.58
46	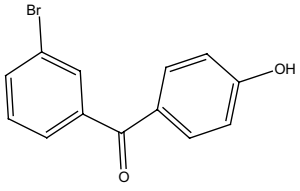 **3-Bromo-4'-hydroxybenzophenone**	−52.71
47	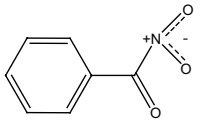 **(o-nitro)-Benzoic acid**	−33.54
48	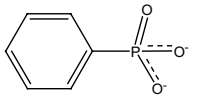 **Phenylphosphonic acid**	−122.64

contacts with active site residues such as Ser136 OG (2.40 Å), His146 NE2 (3.10 Å), Gln137 NE2 (3.72 Å), and Cys138 SG (3.57 Å). Like benzoic acid, compound **48** forms a π-stacking interaction with the imidazole ring of His146 (5.00 Å) and also with the nicotinamide ring of $NADP^+$ (4.10 Å). The hydroxyl group of 4-hydroxybenzophenone (compound **45**) makes hydrogen bond contacts with Gln137 NE2 (3.64 Å) and the main chain nitrogen of Val181 (2.89 Å), while the carbonyl group makes strong van der Waals contacts with Cys138 SG (2.77 Å) and Cys150 SG (3.15 Å). Compound **45** is also within π-stacking distance with the hydroxy group of the catalytic residue of Tyr149 (4.17 Å).

Of the compounds designed by GRID only 4-hydroxybenzophenone was readily and commercially available. The compound was a potent inhibitor of human XR with an IC_{50} value of 120 μM. The lack of a carboxylic acid functional group (characteristic of other inhibitors of XR) in 4-hydroxybenzophenone (compound **45**) provides us with a new lead compound for the development of novel inhibitors for XR. Additionally, the bulk size of 4-hydroxybenzophenone may improve the specificity of this compound for human XR compared to smaller benzoic acid derivatives. While not possessing particularly high protein interaction energies, compounds **40**, **41** and **42** may also be useful inhibitors of XR, as phenol compounds containing the halogen bromide have been shown to be active inhibitors of XR (unpublished results). Halogens such as fluorine and chlorine both produced poor levels of contour energies during GRID analysis and were not used to design de novo inhibitors of XR. This is supported by our own results during database mining, which showed that the potency of nicotinic acid and benzoic acid were diminished when they included a fluoro or chloro functional group. The shallow active site of XR is another positive aspect for compounds **40**, **41** and **42** as their relatively small size, compared to other bulkier inhibitors, suggests that the addition of multiple probes is possible.

3. Conclusion

The use of the NCI database in an efficient computer-based docking system has led to the discovery of two groups of compounds and their derivatives that actively inhibit human XR. They include nicotinic acid (IC_{50} = 100 μM) and benzoic acid (IC_{50} = 29 μM). These results extend and improve upon the activities of known commercially available inhibitors that include aliphatic fatty acids previously discovered for XR[2]. While large database searches are useful in finding new inhibitors of enzymes, the de novo design of compounds using molecular modelling techniques based on established inhibitors prove to also be an effective tool in optimising inhibitor–protein interactions (with the desired active site residues). Used in conjunction with database docking, we have widened the scope of potential inhibitors with likely activity for XR, which was demonstrated through the identification of 4-hydroxybenzophenone (IC_{50} = 120 μM). Molecular modelling and database docking has also identified interactions of several

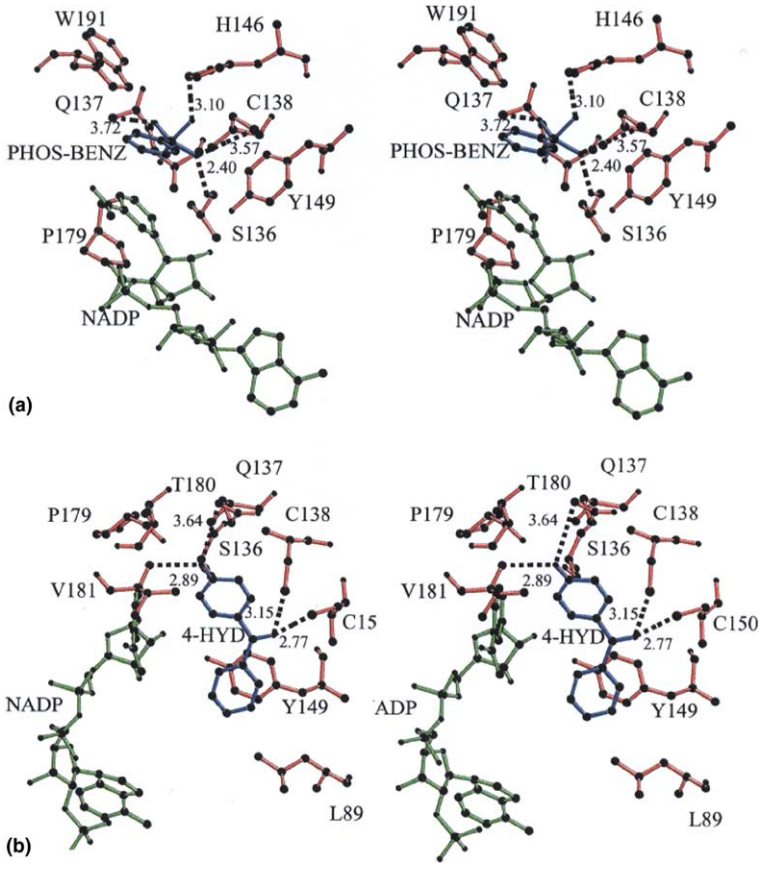

Figure 4. (a) Stereoview picture of phenylphosphonic acid (compound **48**, blue) modelled into the active site of human XR with $NADP^+$ (green) as the co-enzyme. (b) Stereoview of 4-hydroxybenzophenone (compound **45**, blue) modelled into the active site of human XR with $NADP^+$ (green) as the co-enzyme. Figures were generated following molecular dynamics calculations. Residues (red) within 4 Å of ligands are shown. Hydrogen bonds between the ligands and the residues of the active site and their corresponding distances in Å are also shown. The figures were prepared using MOLSCRIPT.[41]

residues, including Gln137 and His146, necessary for successful inhibitory activity and possibly substrate metabolism.

4. Experimental

4.1. NCI database mining

The freely available National Cancer Institute database containing 249,071 organic and inorganic structures[24,38] was downloaded from the website http://cactus.nci.nih.gov/ncidb2/download.html in 3D SDF-File format and then converted to mol2 format using the program Molkit (version 0.91). To easily manipulate the database files and the results garnered from them, the 3D structures were divided up into 249 lots of 1000 and processed individually. The compounds were docked into the active site of the crystal structure of human XR,[27] using the multiple and flexible ligands option in DOCK (Version 4.0).[26,29] SPHGEN, a program supplied with DOCK, was used to identify where ligand atoms may be located within the defined active site region. The compounds that successfully docked into the active site of XR and interacted with the C4 carbon of $NADP^+$ and the catalytic residues of Tyr149 and Ser136, were then selected and viewed in InsightII. Bonds were verified and hybridisation states and charges to functional groups such as the carboxylate and guanidino groups were assigned so as to allow for the accurate configuration of force field potentials for each structure. The docking process was then repeated and the top 250 structures (based on DOCK energy scores and proximity to catalytic residues) were investigated on the CAC-TVS browser (http://131.188.127.153/services/ncidb2).[25] Commercially available compounds were then purchased and evaluated as inhibitors for XR.

4.2. Energy calculations

Energy minimisation and molecular dynamics calculations were carried out using the Discover 2.7 package (Biosym Technologies, San Diego, CA, USA) on an O2 (R12000) workstation (Silicon Graphics, Mountain View, CA, USA) following previously established procedures.[39,40] Minimisation calculations were initiated to relieve any steric hindrance associated with the docked compounds. Calculations were carried out to maximum atomic root-mean-square derivatives of 10.0 and 0.01 kcal/Å using the algorithms steepest descent and conjugate gradient, respectively. To prevent dynamic calculations from being carried out in vacuum and altering significantly the relative positions of the residues, an aqueous environment around the active site was created

using the SOAK (15 Å radius) option in InsightII. Molecular dynamics was performed using the leapfrog algorithms in Discover. Dynamics were equilibrated for 2 ps with time steps of 1 fs and then continued for 4 ps with time steps of 2 fs at 320 K. Finally, the resulting structures were extracted and energy minimised.

4.3. GRID

The program GRID (version 18)[28] was used to search the active site of the enzyme for the most appropriate positions for a variety of probes, as previously described.[44] Briefly, 25 independent probes, which included a variety of functional groups and ions, were used to search the active site of XR for their most favourable positions. The corresponding contour maps were visualised using the contour facility of the InsightII package version 2.1 (Biosym Technologies Inc., San Diego, CA, USA). Calculations were performed on a sphere (15 Å radius) centred on the active site, with a grid spacing of 1 Å. The interaction energy between the probe and every atom within the protein structure was evaluated at each grid point. A dielectric constant of 80 was used to simulate a bulk aqueous phase, while areas as determined by GRID to be excluded from the solvent were assigned a dielectric constant of 4 (i.e., the interior of the protein). The accompanying program GRIN was used to automatically assign atom types and charges for the protein using the standard parameter file provided with GRID. The output was converted (using GINS supplied with GRID) into a form suitable for input to the Biosym utility contour. Contour maps were built using steps of 1 or 0.5 kcal/mol, where negative energy levels depict regions where ligand binding is most favourable and positive energy levels define the surface of the target. The contour map was then superimposed on the active site of the XR model using Insight II. Superposition of the inhibitor onto the active site of XR provided information on the predicted position of the probes. The designed compounds were then docked manually in the active site of XR based on the orientation of the modelled inhibitors so that each probe would be placed in its corresponding favoured region of interaction and energy minimisation and molecular dynamics calculations were then carried out.

4.4. Protein expression

The protein was developed using cDNA coding for the protein and amplified using reverse transcription PCR. Protein expression was carried out in *E. coli* BL21 (DE3) cells and purified using previously described techniques.[2]

4.5. Inhibitory assay for XR

The ability for compounds discovered during database mining to inhibit XR was investigated by evaluating the inhibition of the enzyme activity in vitro. XR activity was measured at 25 °C by monitoring the rate of NADPH oxidation at 340 nm using an Ultrospec 2000 spectrophotometer (Pharmacia Biotech). The standard reaction mixture for the activity assay consisted of 0.1 M potassium phosphate, pH 7.0, 0.1 mM NADPH, 5 mM diacetyl, purified enzyme and inhibitor, in a total reaction volume of 1.0 mL. Most inhibitors were used as aqueous solution. The compounds insoluble in water were solubilised in methanol, and were added to the reaction mixture, in which the methanol concentration was less than 2.5% so as to minimise any inhibitory effect of methanol on the enzyme activity. IC_{50} values (inhibitor concentration resulting in 50% enzyme inhibition) represents the mean of three determinations for each inhibitor.

Acknowledgements

This work was supported in part by an Australian Research Council Linkage International Award (to O.E.K. and A.H.).

References and notes

1. Arsenis, C.; Touster, O. *J. Biol. Chem.* **1969**, *244*, 3895.
2. Nakagawa, J.; Ishikura, S.; Asami, J.; Isaji, T.; Usami, N.; Hara, A.; Sakurai, T.; Tsuritani, N.; Oda, K.; Takahashi, M.; Yashimoto, M.; Otsuka, N.; Kitamura, K. *J. Biol. Chem.* **2002**, *277*, 17883.
3. Ishikura, S.; Isaji, T.; Usami, N.; Kitahara, K.; Nakagawa, J.; Hara, A. *Chem. Biol. Interact.* **2001**, *879*, 130–132.
4. Touster, O.; Hutcheson, R. M.; Rice, L. *J. Biol. Chem.* **1954**, *215*, 677.
5. Touster, O.; Reynolds, V. H.; Hutcheson, R. M. *J. Biol. Chem.* **1955**, *221*, 697.
6. Sochor, M.; Baquer, N. Z.; Mclean, P. *Biochem. Biophys. Res. Commun.* **1979**, *86*, 32.
7. Winegrad, A. I.; Burden, C. L. *N. Engl. J. Med.* **1966**, *274*, 298.
8. Hollmans, S.; Touster, O. In *Non-Glycolytic Pathways of Metabolism of Glucose*; Academic: New York/London, 1964; pp 107–113.
9. Cohn, G. L.; Hume, M. *J. Clin. Invest.* **1960**, *39*, 1584.
10. Spiro, R. G. *N. Engl. J. Med.* **1969**, *281*, 1043.
11. Spiro, R. G.; Fukushi, S. *J. Biol. Chem.* **1969**, *244*, 2049.
12. Sochor, M.; Kunjara, S.; Greenbaum, A. L.; Mclean, P. *J. Dev. Physiol.* **1989**, *12*, 135.
13. Otsuka, M.; Mine, T.; Ohuchi, K.; Ohmori, S. *J. Biochem. (Tokyo)* **1996**, *119*, 246.
14. Thornalley, P. J. *Gen. Pharmacol.* **1996**, *27*, 565.
15. Ortwerth, B. J.; James, H.; Simpson, G.; Linetsky, M. *Biochem. Biophys. Res. Commun.* **1998**, *245*, 161.
16. Spiro, R. G. *Diabetologia* **1976**, *12*, 1.
17. Dyer, D. G.; Dunn, J. A.; Thorpe, S. R.; Bailie, K. E.; Lyons, T. J.; McCance, D. R.; Baynes, J. W. *J. Clin. Invest.* **1993**, *91*, 2463.
18. DesJarlais, R. L.; Seibel, G. L.; Kuntz, I. D.; Furth, P. S.; Alvarez, J. C.; Ortiz de Montellano, P. R.; DeCamp, D. L.; Babe, L. M.; Craik, C. S. *Proc. Natl. Acad. Sci. U.S.A.* **1990**, *87*, 6644.
19. Poroikov, V. V.; Filimonov, D. A.; Ihlenfeldt, W. D.; Gloriozova, T. A.; Lagunin, A. A.; Borodina, Y. V.; Stepanchikova, A. V.; Nicklaus, M. C. *J. Chem. Inf. Comput. Sci.* **2003**, *43*, 228.
20. Lyne, P. D. *Drug Discov. Today* **2002**, *7*, 1047.
21. Walters, W. P.; Stahl, M. T.; Murcko, M. A. *DDT* **1998**, *3*, 160.
22. Korcok, M. *Can. Med. Assoc. J.* **1985**, *133*, 225.

23. Milne, G. W.; Nicklaus, M. C.; Driscoll, J. S.; Wong, S.; Zaharevitz, D. *J. Chem. Inf. Comput. Sci.* **1994**, *34*, 1219.
24. Voigt, J. H.; Bienfait, B.; Wang, S.; Nicklaus, M. C. *J. Chem. Inf. Comput. Sci.* **2001**, *41*, 702.
25. Ihlenfeldt, W. D.; Voigt, J. H.; Bienfait, B.; Oellien, F.; Nicklaus, M. C. *J. Chem. Inf. Comput. Sci.* **2002**, *42*, 46.
26. Shoichet, B. K.; Kuntz, I. D. *Protein Eng.* **1993**, *6*, 723.
27. El-Kabbani, O.; Ishikura, S.; Darmanin, C.; Carbone, V.; Chung, R. P.; Usami, N.; Hara, A. *Proteins* **2004**, *55*, 724.
28. Goodford, P. J. *J. Med. Chem.* **1985**, *28*, 849.
29. Ewing, T. In *DOCK manual version 4.0;* Ed.; University of California: CA, 1998.
30. Ishikura, S.; Isaji, T.; Usami, N.; Nakagawa, J.; El-Kabbani, O.; Hara, A. *Chem. Biol. Interact.* **2003**, *543*, 143–144.
31. Carbone, V.; Darmanin, C.; Ishikura, S.; Hara, A.; El-Kabbani, O. *Bioorg. Med. Chem. Lett.* **2003**, *13*, 1469.
32. Nair, B. *Int. J. Toxicol.* **2001**, *20*, 23.
33. Nasseri-Sina, P.; Hotchkiss, S. A.; Caldwell, J. *Food. Chem. Toxicol.* **1997**, *35*, 409.
34. Pagella, J. H.; Chen, X. B.; MacLeod, N. A.; Orskov, E. R.; Dewey, P. J. *Br. J. Nutr.* **1997**, *77*, 577.
35. Krahenbuhl, L.; Reichen, J.; Talos, C.; Krahenbuhl, S. *Hepatology* **1997**, *25*, 278.
36. Gregus, Z.; Fekete, T.; Halaszi, E.; Gyurasics, A.; Klaassen, C. D. *Drug. Metab. Dispos.* **1998**, *26*, 1082.
37. Lednicer, D. In *Strategies for Organic Drug Synthesis and Design*; Wiley-Interscience: New York, 1998; pp 31–32.
38. Shi, L. M.; Fan, Y.; Lee, J. K.; Waltham, M.; Andrews, D. T.; Scherf, U.; Paull, K. D.; Weinstein, J. N. *J. Chem. Inf. Comput. Sci.* **2000**, *40*, 367.
39. Darmanin, C.; El-Kabbani, O. *Bioorg. Med. Chem. Lett.* **2000**, *10*, 1101.
40. Darmanin, C.; El-Kabbani, O. *Bioorg. Med. Chem. Lett.* **2001**, *11*, 3133.
41. Kraulis, P. J. *J. Appl. Crystallogr.* **1991**, *24*, 946.